Analytical Methods

ROYAL SOCIETY OF CHEMISTRY

CRITICAL REVIEW

View Article Online
View Journal | View Issue

Cite this: *Anal. Methods*, 2024, **16**, 2177

Analysing micro- and nanoplastics with cutting-edge infrared spectroscopy techniques: a critical review

Junhao Xie, *[a] Aoife Gowen,[a] Wei Xu[b] and Junli Xu[a]

The escalating prominence of micro- and nanoplastics (MNPs) as emerging anthropogenic pollutants has sparked widespread scientific and public interest. These minuscule particles pervade the global environment, permeating drinking water and food sources, prompting concerns regarding their environmental impacts and potential risks to human health. In recent years, the field of MNP research has witnessed the development and application of cutting-edge infrared (IR) spectroscopic instruments. This review focuses on the recent application of advanced IR spectroscopic techniques and relevant instrumentation to analyse MNPs. A comprehensive literature search was conducted, encompassing articles published within the past three years. The findings revealed that Fourier transform infrared (FTIR) spectroscopy stands as the most used technique, with focal plane array FTIR (FPA-FTIR) representing the cutting edge in FTIR spectroscopy. The second most popular technique is quantum cascade laser infrared (QCL-IR) spectroscopy, which has facilitated rapid analysis of plastic particles. Following closely is optical photothermal infrared (O-PTIR) spectroscopy, which can furnish submicron spatial resolution. Subsequently, there is atomic force microscopy-based infrared (AFM-IR) spectroscopy, which has made it feasible to analyse MNPs at the nanoscale level. The most advanced IR instruments identified in articles covered in this review were compared. Comparison metrics encompass substrates/filters, data quality, spatial resolution, data acquisition speed, data processing and cost. The limitations of these IR instruments were identified, and recommendations to address these limitations were proposed. The findings of this review offer valuable guidance to MNP researchers in selecting suitable instrumentation for their research experiments, thereby facilitating advancements in research aimed at enhancing our understanding of the environmental and human health risks associated with MNPs.

Received 12th October 2023
Accepted 15th March 2024

DOI: 10.1039/d3ay01808c

rsc.li/methods

1. Introduction

Microplastics (MPs) are commonly defined as plastics with the largest dimension of <5 mm. In contrast, there is no consensus on the definition of nanoplastics (NPs). Several studies define NPs as particles with a diameter of <1 μm.[1,2] In this review, we will adopt this definition for NPs, and collectively refer to MPs and NPs as MNPs. MNPs, as emerging pollutants, are ubiquitously present in marine environments,[3] terrestrial ecosystems,[4] drinking water,[5] and even human bodies.[6] With the rapid growth of research on MNPs in recent years, the global distribution of them has become evident. While some studies have indicated that these minuscule plastic particles can have adverse effects on organisms,[7] the knowledge regarding the impact on human health is still limited. To accurately assess the hazards posed by these emerging pollutants, reliable analysis of them is critical.

Early analysis of plastic particles was often based on visual inspection (with the naked eye or a microscope), a method that is no longer accepted mainly due to its subjectivity in particle selection, lack of chemical specificity (or low chemical specificity when hot needles or Nile red dye was used), time-consuming and laborious nature, and inability to provide information on the chemical composition of particles.[8] Consequently, this strategy has been largely replaced by methods that are convenient and could identify the chemical composition. Infrared (IR) spectroscopy is one of such methods and is advantageous compared to several other methods that could identify the polymer type. For instance, unlike pyrolysis-gas chromatography coupled to mass spectrometry, IR spectroscopy is non-destructive, hence the morphological information of plastic particles is not lost.[8] Furthermore, in comparison to Raman spectroscopy, IR spectroscopy is rarely associated with fluorescence interference – a crucial attribute, especially when analysing weathered plastic particles or plastic particles with pigment additives.[9]

[a]*School of Biosystems and Food Engineering, University College Dublin, Belfield, Dublin 4, Ireland. E-mail: junhao.xie@ucdconnect.ie; Tel: +353 872315465*
[b]*Department of Life Sciences, Center for Coastal Studies, College of Sciences, Texas A&M University-Corpus Christi, USA*

In recent years, with advancements in technology, IR spectroscopy has evolved into a broader category, encompassing not only the well-established Fourier transform infrared (FTIR) spectroscopy but also emerging techniques like quantum cascade laser infrared (QCL-IR) spectroscopy, atomic force microscopy-based infrared (AFM-IR) spectroscopy, and optical photothermal infrared (O-PTIR) spectroscopy. Among these IR spectroscopic techniques, FTIR spectroscopy was the earliest technique applied to the analysis of MPs. While standalone FTIR spectrometers might suffice for the analysis of large MPs (*e.g.*, >500 μm), when dealing with small MPs (*e.g.*, <500 μm), the use of a microscope, in addition to an FTIR spectrometer, becomes necessary. This combined approach involving both a microscope and an FTIR spectrometer is commonly referred to as micro-FTIR (μ-FTIR). With the application of focal plane array FTIR (FPA-FTIR), the data collection speed for MP analysis is significantly improved, and unbiased analysis could be achieved, since no manual presorting of particles is needed. Hence, FPA-FTIR has been considered to have tremendous potential in the automated analysis of MPs.[10] Subsequently, advanced IR spectroscopy techniques, namely, QCL-IR spectroscopy, AFM-IR spectroscopy, and O-PTIR spectroscopy were applied for MNPs analysis,[11–13] with each demonstrating great potentials. These IR spectroscopic techniques are based on distinct principles. A comprehensive understanding of the principles, advantages, and limitations of these IR spectroscopic techniques is crucial for conducting reliable MNP research with them. Therefore, a paper summarising the application of these IR spectroscopic techniques and their relevant instruments in MNP analysis would be of great interest to readers.

To this end, the objectives of this review article are (1) to investigate the application of the state-of-the-art IR techniques in MNP research over the past three years, (2) to compare instruments built from different IR spectroscopic techniques in terms of substrates/filters, data quality, spatial resolution/detection limit, analysis speed, data processing, cost, and *etc.*, and (3) to identify limitations of certain IR instruments and provide recommendations for future applications.

1.1. Fundamentals of IR spectroscopic techniques

1.1.1. FTIR spectroscopy. FTIR spectroscopy studies the interaction between matter and IR radiation. Following this interaction, the residual IR radiation is recorded to generate a spectrum, which reveals the specific chemical bonds present in the sample. The source of IR photons in an FTIR instrument is typically a thermal Globar. The interferometer is a key component of an FTIR instrument, and it creates an interferogram as the raw signal. This signal is then "Fourier transformed" into an actual spectrum, revealing the chemical composition of the sample. In MP analysis with FTIR spectroscopy, three modes are commonly employed: transmission, reflection (*i.e.*, transflectance and diffuse reflection), and attenuated total-reflectance (ATR), each having different applicable situations. In transmission mode, the IR radiation that passes through the sample is measured by the detector. Hence, the transmission mode is suitable for relatively thin samples or samples with weak IR absorption, and, in the case of MP detection, an IR transparent substrate/filter is needed. In transflectance mode, IR radiation is passed through the sample, reflected off an IR reflective substrate and back though the sample a second time and onto the detector. This mode is suitable for thin samples as well and requires an IR reflective substrate or filter, but its suitability also depends on the morphology of the sample, which could cause light scattering and disturb the reflected signal. In diffuse reflection (DRIFTS) mode, IR radiation interacts with the MP particles and reflects off their surfaces, causing the light to diffuse or scatter as it travels through the sample. The scattered energy is then directed to the detector through an output mirror to generate a spectrum. DRIFTS mode is commonly used for analysing powdered MPs and requires a DRIFTS accessory.[14] In ATR mode, the generation of spectra relies on contact between an ATR crystal and the sample. When the ATR crystal and the sample are in close contact, IR light is sent in and bounces through the crystal, creating evanescent waves before it is collected on the other side. Information about the sample is gathered through the interaction of the evanescent waves and the sample. ATR mode is commonly used for analysing thick or strong-IR-absorbent samples.[15] While ATR mode minimises sample preparation, there are concerns of it: first, the crystal itself is expensive and degrades over time. Secondly, since the ATR crystal needs to come into contact with the sample, it may cause cross-contamination and sample loss. Finally, analysing samples smaller than the ATR crystal may result in low quality spectra.[16]

μ-FTIR can effectively analyse single MP particles smaller than 500 μm, a task that could be challenging to achieve using standalone FTIR spectrometers. Therefore, with the current trend of analysing smaller MPs, μ-FTIR might be preferred. In early (from 2004 to around 2012) detection of MPs, the μ-FTIR systems used were equipped with a single-element (IR) detector only, this means that only one FTIR spectrum could be obtained at a single point on the sample at a time. While using a single-element detector in combination with a motorised stage allows for the collection of spatial and spectral information (*i.e.*, chemical imaging) of MP samples, the imaging speed is significantly slow. Subsequently, the introduction of line array detectors, where several single-element detectors are arranged in a line, has enabled the simultaneous collection of multiple spectra within a single line. By employing a line array detector and a motorised stage to collect data from multiple rows, chemical images could be rapidly generated. The most advanced detector for μ-FTIR is the FPA detector, consisting of an array of IR detectors arranged in a square pattern (*e.g.*, 64 × 64 detectors, 128 × 128 detectors). An FPA detector allows for the simultaneous collection of spectral data from multiple points on a single plane. Consequently, when coupled with a motorised stage, the imaging speed is greatly enhanced. The amount of data that can be collected simultaneously depends on the size of the FPA. For instance, an FPA with a size of 64 × 64 can acquire 4096 (64 × 64 = 4096) spatially resolved spectra in a single acquisition. FPA-FTIR has demonstrated tremendous potential in the field of automated MP analysis.[17]

1.1.2. QCL-IR spectroscopy. Similar to FTIR, QCL-IR spectroscopy also measures the residual IR radiation produced from the interaction of IR light with the sample to generate a spectrum; however, in contrast to the thermal sources commonly used in FTIR spectroscopy, QCL-IR spectroscopy employs a QCL as the IR radiation source. Unlike thermal IR sources, which emit diffused IR radiation over a broad spectral range (typically between 4000–400 cm^{-1} in MP research), QCLs can produce coherent IR radiation at specific and selectable wavelengths. The high brilliance of QCL radiation allows for a more focused and intense beam, leading to improved signal-to-noise ratios (SNR). The greater spectral power density of QCLs is however, accompanied by a trade-off – a reduced spectral range, which posed significant limitations for early QCLs. Fortunately, advancements in technology have led to the development of QCLs capable of covering the full molecular fingerprint spectral region today. In quantum cascade structures, electrons undergo intersubband transitions, leading to the emission of photons. The electrons tunnel to the next period of the structure, and this process repeats. As a result, unlike IR interferometers, QCLs generate the mid-IR signal wavelength-by-wavelength in absolute values, eliminating the need for Fourier transform for spectrum reconstruction.[18] QCL-IR instruments can operate in transmission, reflection, and ATR modes, and the applicability of each mode is similar to that of FTIR.

In MP analysis, the feature of tunability (of the IR frequency) of the QCL-IR technique allows the IR light to solely focus on the specific and optimal IR range and hence allows rapid identification of known types of MPs. Furthermore, this feature enables the direct generation of single frequency images. This is in stark contrast to FTIR spectroscopy, where the IR range cannot be manually adjusted, and therefore, acquiring single frequency images requires a significant amount of time to first acquire hyperspectral images.

Currently, two QCL-IR spectroscopy-based approaches have been employed in the field of MP research. One utilises a single-element detector in conjunction with a fully automated MP detection workflow, while the other employs a large FPA (480 × 480) detector.[19] While the combination of an FPA detector and a QCL significantly improves the efficiency (due to super-fast imaging speed) in data collection,[11] using an FPA detector in a QCL system may pose a risk of laser coherence artefacts in the acquired images or spectra.[20]

1.1.3. O-PTIR spectroscopy. O-PTIR spectroscopy is an advanced spectroscopic technique that allows spectral information at a submicron scale to be obtained.[21] Unlike FTIR spectroscopy or QCL-IR spectroscopy, O-PTIR spectroscopy does not measure residual IR radiation. Instead, it measures the sample's intrinsic IR absorption. The O-PTIR technique acquires spectral information through an innovative "pump–probe" architecture (Fig. 1). During operation, the tunable IR laser (*e.g.*, a QCL), acts as the pump, while the visible laser (532 nm or 785 nm) serves as the probe, both co-linearly illuminating the sample. The pump, by adjusting its own IR frequency, excites the sample and induces a photothermal IR effect, resulting in transient thermal expansion and changes in the sample's refractive index. These changes in refractive index are then detected by the probe. The probed information, varying with the IR frequency, is used to generate an O-PTIR spectrum. O-PTIR spectra closely resemble conventional FTIR spectra,[13] allowing for comparisons with FTIR spectral libraries. However, the quality of O-PTIR spectra is superior because the O-PTIR technique is immune to dispersive scatter artefacts,[22] which can often compromise the quality of FTIR or QCL-IR spectra. Regarding the spectral range, the spectral coverage of the O-PTIR technique depends on the IR laser(s) it is paired with. When a standard QCL is used, a spectral range of ~1800 to ~800 cm^{-1} is covered. If the laser source is a dual-range (C-H/FP) QCL, not only ~1800 to ~800 cm^{-1}, but also the C–H stretch range −3000 to 2700 cm^{-1}, are covered. When use a combination of a standard QCL and an optical parametric oscillator (OPO), the covered ranges are 3600–2700 cm^{-1} and 1850–800 cm^{-1} in a single unit.

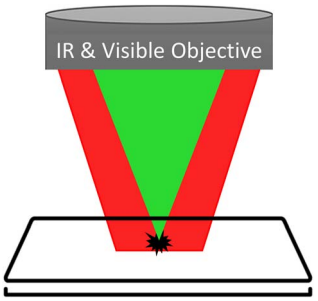

Fig. 1 The "pump–probe" structure of the O-PTIR technique. The sample is illuminated by both the pump (red light) and the probe (green light). The pump, by modulating its IR frequency, induces a photothermal IR effect in the sample, which is then detected by the probe.

Currently, commercially available O-PTIR microscopes offer the capability to collect optical images (Fig. 2a), single frequency images (Fig. 2b), visible-laser images (Fig. 2c), point spectra (Fig. 2d) and hyperspectral images for MNP analysis, providing morphological and chemical information. However, a significant limitation exists in current O-PTIR microscopes, as they are equipped with a single-element detector only, which means that the imaging speed is greatly restricted.

It is worth mentioning that with the O-PTIR technique, it is possible to collect both O-PTIR spectra and Raman spectra at the same point and time. This feature can provide more reliable identification results for MNP research compared to obtaining IR or Raman spectra alone.[23] But this review only focuses on IR techniques, so the capability of O-PTIR spectroscopy to acquire Raman spectra is not further discussed.

1.1.4. AFM-IR spectroscopy. AFM-IR spectroscopy, as the name suggests, is a combination of AFM and IR spectroscopy. Specifically, AFM-IR spectroscopy represents a remarkable integration of AFM's exceptional spatial resolution and the chemical analysis capabilities offered by IR spectroscopy.[24] The spatial resolution of AFM-IR spectroscopy is approximately 20 nm, and the resolution is only limited by the radius of the apex of the AFM probe tip. As a result, this technique has the potential to identify plastic particles at the nanometre level. The

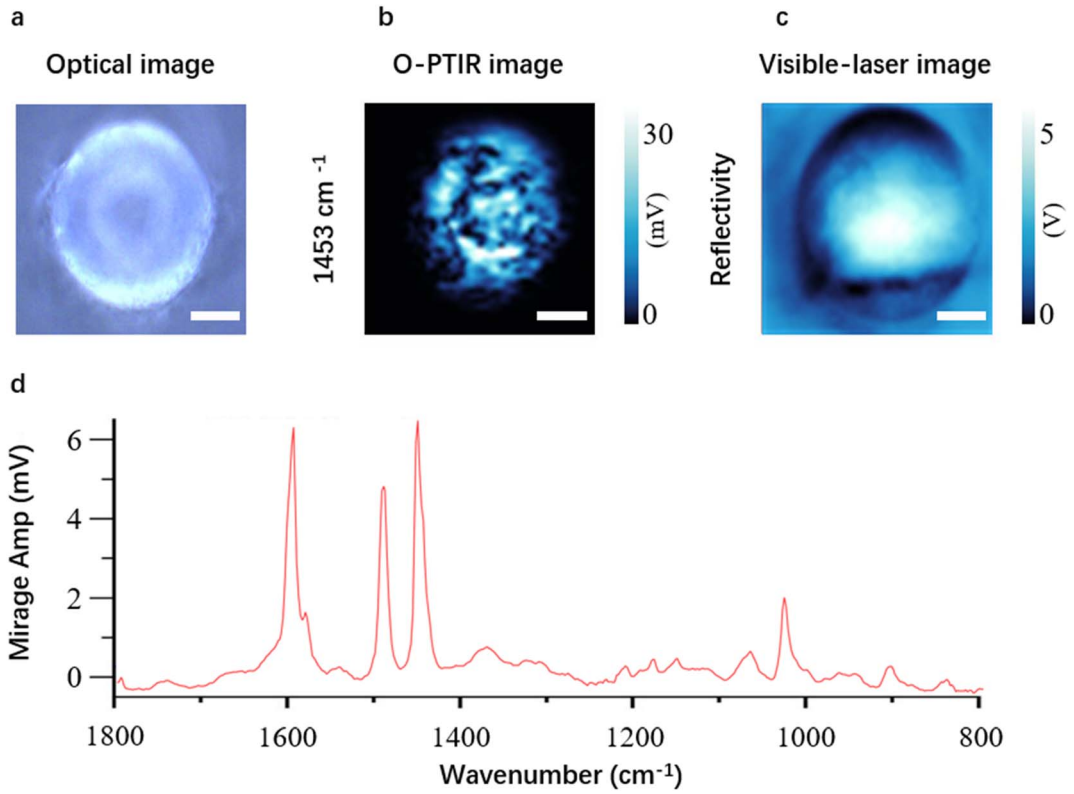

Fig. 2 An optical image (a), a single frequency image at 1453 cm^{-1} (b), a visible-laser image (c), and a spectrum of a polystyrene (PS) microbead (d) placed on a glass slide acquired using our in-house mIRage O-PTIR microscope. A single frequency image obtained with the O-PTIR technique is often referred to as an O-PTIR image. 1453 cm^{-1} is the band where PS shows one of its characteristic peaks. The white scale bar is 20 μm. The colour scales show the signal intensity.

working principle of the AFM-IR technique is very similar to that of the O-PTIR technique, as both are based on the photothermal effect induced by IR radiation on the sample. The main difference lies in the detection of the photothermal effect, where the O-PTIR technique employs a laser beam as the probe, while the AFM-IR technique uses an AFM cantilever as the detection probe. Fig. 3 is a schematic diagram of the AFM-IR technique, which shows how spectral information is acquired using this technique. A tunable IR laser (*e.g.*, a QCL or an OPO) is focused on a specific region of a sample near the tip of an AFM cantilever probe. When the tunable IR laser is set to a wavelength that corresponds to an absorbing wavelength of the sample, the sample's photothermal IR effect is induced, leading to transient thermal expansion. This thermal expansion causes a force impulse on the tip of the cantilever, resulting in an oscillation of the AFM cantilever. By recording the AFM cantilever oscillation amplitude as a function of wavelength (or wavenumber), a local absorption spectrum of the sample can be generated.[25] Additionally, it is possible to lock the IR frequency at a predetermined wavelength to generate single frequency images.[25] In MNP research, AFM-IR spectroscopy is not only used for particle identification but also for the characterisation of the microstructure/nanostructure of the MNP surface.

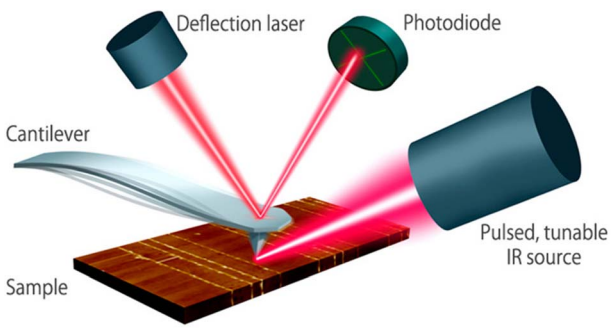

Fig. 3 Schematic diagram of the AFM-IR technique. A pulsed tunable laser is directed towards the part of the sample close to the tip of an atomic force microscope. By tuning the laser to a specific absorbing wavelength of the sample, the IR radiation gets absorbed, leading to photothermal expansion in the absorbing regions of the sample. The tip of the cantilever serves as a detector to measure local IR absorption. Adapted with permission from Dazzi and Prater.[25] Copyright 2023 American Chemical Society.

1.2. MNP analysis with IR spectroscopic techniques

MNP samples from the environment are complex cocktails that not only contain MNPs but also various substances such as tissues, cellulose, chitin, silica, minerals. The presence of such organic and inorganic materials in the sample significantly affects the MNP analysis as the signal of these materials might overlay MNP spectra. Therefore, applying effective methods to

extract MNPs from the environmental matrix before IR spectroscopic analysis is essential. The extraction of MNPs typically involves the digestion of organic materials and the removal of inorganic materials (usually by density separation). Examples of MNP extraction, as well as the major reagents/methods used are detailed in Section 3.1.1 of this article.

The separation of MNPs from environmental matrices is often considered a necessary step. However, some researchers might apply an IR spectroscopic technique to directly image the sample matrix for the purpose of identifying MNPs mixed in it.[26] In other words, depending on the research question of interest, the extraction of MNPs from a matrix may not be necessary.

If the research question of interest is to explore the effects of a treatment on MNPs, the MNPs might be intentionally treated (*e.g.*, oxidised) before IR spectroscopic analysis.

Subsequently, the extracted MNPs, or samples containing MNPs, or treated MNPs are typically enriched on or transferred to a substrate/filter, getting ready for IR spectroscopic analysis.

For the detection of MNPs using IR spectroscopy, there are two widely adopted methods. The first one is hyperspectral imaging (Fig. 4a), where a spectrum for every "pixel" in the region of interest is collected. Individual pixels are then classified based on their spectral signatures. The second approach is particle-based analysis (Fig. 4b), where all particles in a region of interest are first located. Subsequently, the operator collects spectra for each located particle. Then the collected spectra are classified to distinguish which particles are MNPs and which are not. Particle location/recognition can be based on visible light (*e.g.*, manually locating substances that appear as particles to the naked eye or under a microscope); it can also be based on single frequency IR light (see Section 3.1.6 for an example).

A diverse array of algorithms has been developed to classify pixels or spectra, falling into two primary categories: instance-based and model-based machine learning approaches.[27] In instance-based methods, reference data (*i.e.*, instances) are directly employed to identify unknown spectra through similarity assessments. Various methods, such as Pearson correlation analysis and spectral angle mapper (SAM), can be used for similarity assessment. A notable advantage of instance-based approaches lies in their adaptability, as the spectroscopic reference data can be easily expanded or customised, for instance, by incorporating pertinent spectra into the existing spectral library.[27] However, it should be noted that these methods can result in a significant computational burden and are time-consuming due to the necessity of computing similarities between each collected spectrum and every reference spectrum in the library. In contrast, model-based approaches rely on statistical models trained from spectroscopic reference data (*e.g.*, partial least squares-discriminant analysis (PLS-DA) models, support vector machine (SVM) models, and random decision forest (RDF) classifiers), which are then applied to unknown spectra. These unknown spectra are then classified into predefined categories which may encompass polymer types and substances associated with environmental MNP samples. Notably, model-based techniques typically offer shorter analysis times, enabling a higher analytical throughput.[28] Nonetheless, it is imperative to enhance the robustness of these models before their practical application can be fully realised.

Hyperspectral imaging is associated with larger file sizes and time demands (when an array detector is unavailable) since every pixel within the region of interest undergoes spectral acquisition, including pixels devoid of MNPs. Conversely, particle-based analysis selectively gathers spectra from particles only, resulting in reduced data storage space and time requirements (when the number of particles in the region of interest is relatively low). An inherent advantage of hyperspectral image analysis lies in its capacity to provide accurate particle characterisation including both chemical composition and physical properties such as size and shape. In contrast, particle-based analysis often involves collecting one to several spectra from a particle solely for identification purposes. If precise information on particle size and shape is desired,

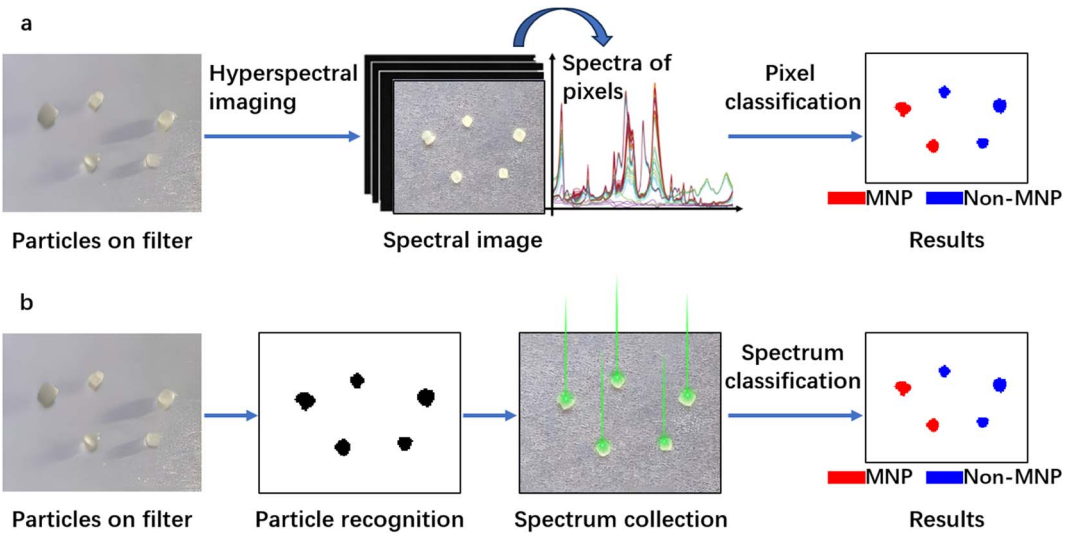

Fig. 4 Detection of particles through hyperspectral imaging (a) and through particle-based analysis (b).

complementary image analysis methods need to be employed. Both approaches ensure the chemical identification of observed particles, thereby providing reliable outcomes. Without the utilisation of these two approaches (or other effective approaches) for chemical identification, the quantification of MNP particles would yield inaccurate results. For instance, Hernandez *et al.*[29] directly labelled particle-like substances observed under a scanning electron microscope as MNPs, without subjecting them to proper chemical identification. As a consequence, their results have faced criticism.[30]

2. Literature review methodology

A literature search on Scopus (**https://www.scopus.com**) was conducted to gather information about the IR techniques and instruments used in recent years in MNP research. The keywords used for the search were "IR OR infrared" and "microplastic*", and these were searched within the Article title, Abstract, and Keywords. The search was conducted on April 13, 2023. The results obtained were first filtered on the Scopus website using the following criteria: the year of publication was limited to "2023", "2022", and "2021"; the document type was limited to "Article"; the publication stage was limited to "Final"; and the language was limited to "English". A database was then formed, containing the retained articles, one paper published in 2020 that describes the combination of QCL-IR spectroscopy with a large FPA detector for MP monitoring, and three studies related to O-PTIR spectroscopy for MNP research but unavailable on Scopus.

The published work in the database was then accessed one by one. Through reading the titles, abstracts, and parts of the text, the literature was further screened according to the following exclusion criteria: articles that could not be accessed, research that did not focused on MP (*e.g.*, focused on bulk plastics), research that did not use IR spectroscopy/instruments and research that did not specify either the brand or the model of the IR instrument used.

3. Results from the literature review

The literature search on Scopus initially yielded 1987 sources. After the first round of screening, 1178 articles were deemed relevant and retained. These 1178 retained articles, along with an additional four relevant articles identified through other sources, were amalgamated to form a database comprising a total of 1182 articles. A second round of screening was then conducted on the database, resulting in a final selection of 988 articles for further analysis.

The findings from the studies covered in this review indicate that FTIR spectroscopy is the most extensively utilised technique in MP research, with 953 studies employing it. Following FTIR spectroscopy, QCL-IR spectroscopy was used in 35 studies, and O-PTIR spectroscopy in six studies. AFM-IR spectroscopy was the least used technique, with only three publications incorporating it. Among these IR techniques, FTIR spectroscopy stands as the oldest technique and has been continuously developed since its introduction in the 1950s.[31–34] The prevalent use of FTIR spectroscopy in MP research can be attributed to its capability to deliver reliable qualitative and quantitative results (and some surface characterisation results through hyperspectral imaging). Additionally, its low costs (compared to instruments based on the newer IR spectroscopic techniques) and early commercial availability (the first commercial FTIR instrument introduced as early as 1969),[32] might have contributed to its widespread adoption. The developmental timeline of FTIR spectroscopy and the introduction of instruments based on the newer IR techniques can be observed in Fig. 5. As seen, instruments based on newer IR spectroscopic techniques have

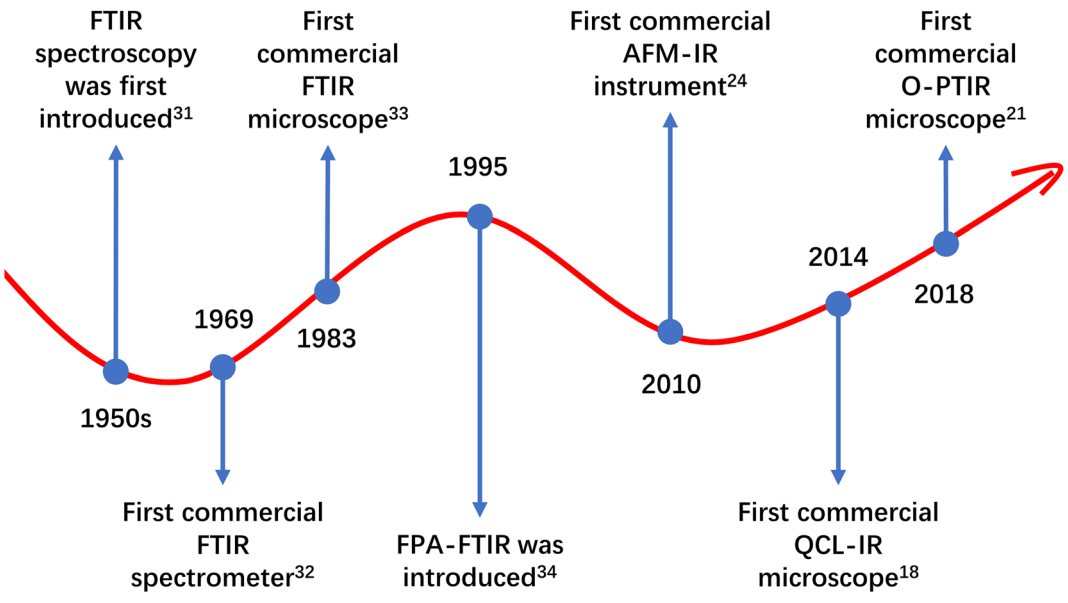

Fig. 5 The developmental timeline of FTIR spectroscopy and the introduction of instruments based on the new IR spectroscopic techniques (O-PTIR spectroscopy, QCL-IR spectroscopy, and AFM-IR spectroscopy).

become commercially available only in the last decade. Despite these new IR spectroscopic techniques having demonstrated greater potential than FTIR spectroscopy in MP research,[11–13] they might not have had sufficient time to become as popular as FTIR spectroscopy. Among the newer IR spectroscopic techniques, O-PTIR spectroscopy and QCL-IR spectroscopy seem to be more favoured by MNP researchers, despite their relevant instrumentation becoming commercially available later than AFM-IR spectroscopy-based instrumentation.

FTIR spectroscopy is widely employed for the analysis of MPs, and it can be implemented using either FTIR spectrometers or μ-FTIR systems. FTIR spectrometers employing ATR have been commonly used for the identification of MPs >500 μm, while μ-FTIR systems are more suitable for identifying MPs <500 μm. Currently, there are numerous models of FTIR instruments used in MP research. The most frequently utilised FTIR instruments in the last three years are listed in Table 1. Instruments that have been used in fewer than 8 studies are not included in this table. Additionally, it is indicated in the table that whether the listed instrument is equipped with a line array detector or an FPA detector, and the number of times these array detectors were used for imaging (instruments equipped with an array detector is also equipped with a single-element detector, allowing users to collect point spectra when analysing MPs, rather than necessarily performing imaging). As evident from Table 1, the most popular FTIR spectrometer is the Nicolet 6700 (Thermo Scientific), used in 44 studies, while the Nicolet iN10 (Thermo Scientific) is the preferred μ-FTIR system, employed in 70 studies. FTIR spectrometers have been used in 508 studies, while μ-FTIR has been used in 255 studies. This observation might suggest that in the past three years, research on MPs >500 μm has been approximately twice as prevalent as research on MPs <500 μm. In addition, the ownership rate of IR instruments equipped with an array detector among MP research teams seems to be low, possibly because instruments with an array detector are more expensive than those with

Table 1 Summary of the usage frequency of FTIR instruments based on studies covered in this review[a]

Instrument and brand	Is μ-FTIR?	Frequency[b]
Nicolet iN10, Thermo Scientific	Yes	70
Nicolet iN10 MX, Thermo Scientific	Yes	45, in which 8 used the line array detector
Nicolet 6700, Thermo Scientific	No	44
Spotlight 400 microscope coupled to a FTIR spectrometer, PerkinElmer	Yes	43, in which 15 used the line array detector
Nicolet iS50, Thermo Scientific	No	42
Spotlight 200 microscope coupled to a FTIR spectrometer, PerkinElmer	Yes	40
Spectrum Two, PerkinElmer	No	40
Vertex70, Bruker	No	39
Cary 630, Agilent	No	39
Nicolet iS5, Thermo Scientific	No	37
Nicolet iS10, Thermo Scientific	No	37
ALPHA, Bruker	No	36
Tensor 27, Bruker	No	29
Spectrum 100, PerkinElmer	No	24
Cary 620 microscope coupled to a FTIR spectrometer, Agilent	Yes	21, in which 17 used the 64 × 64 FPA detector
FT/IR 6000, JASCO	No	19
IRTracer-100, Shimadzu	No	18
IRAffinity-1/S, Shimadzu	No	16
IR Prestige-21, Shimadzu	No	14
Frontier, PerkinElmer	No	14
HYPERION 3000, Bruker	Yes	14, in which 7 used the 64 × 64 FPA detector
HYPERION 2000, Bruker	Yes	14
ALPHA II, Bruker	No	10
Nexus 670, Thermo Scientific	No	9
TENSOR II, Bruker	No	9
Nicolet iS20, Thermo Scientific	No	8
FT/IR 4000, JASCO	No	8
Spectrum ONE, PerkinElmer	No	8
VERTEX 70v, Bruker	No	8
LUMOS II, Bruker	Yes	8, in which 5 used the 32 × 32 FPA detector

[a] The FTIR microscopes listed in this table may be coupled to the FTIR spectrometers also listed in this table. In such cases, the FTIR microscope, when coupled to the FTIR spectrometer, is considered as a single entity of the of FTIR microscope, and its usage is not counted again as the FTIR spectrometer. [b] In this column, if the frequency (number) listed is followed by a sentence, it indicates the instrument is equipped with an FPA detector or a line array detector, and the number of studies (specified in the sentence) these array detectors were used in.

a single-element detector only. Furthermore, even one has an FTIR instrument equipped with an array detector, it does not necessarily mean they need to use the array detector for chemical imaging, as revealed by the data, the usage rate for line array detectors is only 8%, and for FPA detectors, it is 67%. Indeed, if a single-element detector can quickly complete an MP detection task, chemical imaging may not be necessary. For instance, when the number of particles in a region of interest is low, the operator can directly click on each particle and collect spectra without the need for imaging the entire region of interest, which produces a huge amount of data that requires significant computing power and time to process.[35]

In comparison to the numerous models of FTIR instruments used in MP research, there are relatively fewer instrument models available for the other three IR techniques. This review identified two QCL-IR instruments used for MP analysis: the 8700 LDIR (Agilent), employed in 34 studies, and the SPERO microscope (Daylight Solutions), used in one study. The 8700 LDIR is equipped with a single-element detector and comes with specialised software Clarity (Agilent) designed for automated MP analysis. The SPERO microscope is equipped with a large 480 × 480 FPA detector. Under low magnification (4×), it covers a field of view of 2000 μm × 2000 μm and produces a projected pixel size of 4.25 μm. Under high magnification (12.5×), it covers a field of view of 650 μm × 650 μm and generates a projected pixel size of 1.36 μm. For O-PTIR instruments, we found two models: the mIRage microscope (Photothermal Spectroscopy Corp) and the mIRage+R microscope (Photothermal Spectroscopy Corp). These were used in four and two studies, respectively, and both have a single-element detector. For AFM-IR instruments, we identified the Nano IR2 (Anasys Instruments Inc), which was used in three studies.

3.1. Comparisons of IR instruments

In the following section, we will conduct a comprehensive comparison of several cutting-edge IR instruments that have been identified in the studies covered by this review. FPA-FTIR stands out as the most advanced form within the FTIR category, thereby warranting the inclusion of all FPA-FTIR models, namely the Cary 620, the HYPERION 3000, and the LUMOS II, in our comparison. Additionally, the 8700 LDIR and the SPERO microscope, both QCL-IR instruments, as well as the mIRage microscope and the mIRage+ R microscope, which are O-PTIR microscopes, and the Nano IR2, an AFM-IR instrument, will also be included in the comparison.

3.1.1. Application to environmental samples. Table 2 summaries the sample types (in which MNPs were detected) analysed in studies included in the comparison, the IR instruments used, the reagents/methods used for MNP extraction, along with associated recovery rates. It can be seen that MNPs have been detected in a very wide range of environmental matrices. Through further investigation of the sample types listed in Table 2, one might find that the FPA-FTIR microscopes, *i.e.*, the Cary 620, the HYPERION 3000, the LUMOS II and a QCL-IR microscope – the 8700 LDIR have been used for analysing a broader range of sample types, including treated water, sea water, sand, sediment, soil, sludge, slurry, biological samples, and *etc.*; while the SPERO microscope, the O-PTIR microscopes, and the Nano IR2 have been used for fewer sample types. However, it should be noted that there is no evidence suggesting that the FPA-FTIR microscopes and the 8700 LDIR can deal with more sample types while the other instruments listed could not. For analysing a specific sample, the instrument that would be used is likely dependent on the availability of instrumentation in the researcher's laboratory. As discussed, since FPA-FTIR is the earliest developed technique among the IR techniques discussed in this article, it is not surprising that FPA-FTIR microscopes have been acquired by a decent number of laboratories, hence the number of sample types associated with FPA-FTIR is higher. The fact that the 8700 LDIR has been used to analyse a wide range of sample types within just a few years since its release (in 2018) might be attributed to its automated MP analysis software, and its low price (see Section 3.1.7 for instrument cost/price).

3.1.2. Pretreatments, filters/substrates. In the extraction of MNPs from environmental matrices, organic materials were typically digested using strong acidic solutions (*e.g.*, nitric acid), strong alkaline solutions (*e.g.*, potassium hydroxide), oxidation agents (*e.g.*, Fenton's reagent, hydrogen peroxide), enzymes, or a combination of these chemicals. Notably, acidic solutions, alkaline solutions and some oxidation agents have been reported to cause particle losses, for example, certain acids can dissolve some PS, PA, PE and PP,[90] while enzymes are considered mild and, therefore, plastic-conserving.[100] The removal of inorganic materials was typically realised by density separation with solutions of high density, *e.g.*, sodium chloride (NaCl), zinc chloride ($ZnCl_2$), sodium polytungstate (SPT) solutions, *etc.* A good extraction/purification method should have a high recovery rate and low time and labour costs. An example of an effective purification method is the Universal Enzymatic Purification Protocol (UEPP) developed by Löder *et al.*[100] According to UEPP, samples are first incubated with sodium dodecyl sulfate (SDS) to increase the contact surface for enzymatic treatments. Subsequently, enzymatic treatments are carried out sequentially in the optimal environment (created by using buffers and pH adjustment), starting with a protease treatment, followed by a lipase treatment, a cellulase treatment, an amylase treatment, and a chitinase treatment. Before the chitinase treatment, hydrogen peroxide is added to facilitate better contact between the chitinase and chitin. After applying all enzymatic treatments, hydrogen peroxide is used to degrade the remaining organics. The enzymatic treatments are dependent on the chemical composition of the sample matrix (*e.g.*, if the sample matrix does not have chitin in it then a chitinase treatment is not needed). Finally, $ZnCl_2$ is used for density separation to remove inorganic materials. UEPP, due to its high recovery rate and cost-effectiveness,[100] were adopted in multiple studies covered in this review. The cobalt salts(II)/peroxymonosulfate (Co/PMS) system for MNP flotation proposed by Wang, Tan *et al.*[101] is also a noteworthy state-of-the-art approach for MNP extraction or purification. PMS can be effectively activated by cobalt(II) salts,[102] and once activated, it generates reactive species capable of removing a variety of

Table 2 Summary of MNP samples analysed using the IR instruments included in the comparison, along with the major reagents or methods used in sample pretreatment, and associated recovery rates[a]

IR instrument	Sample types	Pretreatment[b]	Size, % recovery, and particle type	Reference
Cary 620	Tap water	Acetic acid to dissolve inorganics	NA	36
	Bottled water	DS: $ZnCl_2$ Citric acid to dissolve remaining inorganics	95–145 μm, 63 ± 8%, PS	37
	Water from drinking water distribution pipes	DS: SPT	NA	38
	Sea water	D: protease, cellulase, Viscozyme, Fenton's reagent DS: SPT	90–106 μm, 90.3 ± 1.1%, PE	39
	Sea water	NA	NA	40
	Sea water	Modified UEPP	90 μm, 75%, PS	41
	Sea water	D: protease, cellulase, Viscozyme, Fenton's reagent DS: SPT	NA	42
	Sand	DS: NaCl	NA	43
	Sediment	D: H_2O_2 DS: $ZnCl_2$	90–180 μm, 42.3 ± 4.4%, PE 100–500 μm, 78.9 ± 6.2%, PS 100–500 μm, 77.6 ± 6.5%, PC	44
	Sediment	D: H_2O_2 DS: LST	250–500 μm, 98%, PET 250 μm, 89%, HDPE	45
	Sediment	DS: NaCl	85 ± 3%, PE, PP, PS, PU 67 ± 3%, PVC, PET	46
	Soil	DS: NaCl, $ZnCl_2$	NA	47
	Fatty slurries, grease, sewage sludge, digested sludge from WWTP digesters	D: lipase, cellulase, protease, H_2O_2, Fenton's reagent DS: SPT	NA	48
	GITs of fish	UEPP	90 μm, 75.0 ± 10.0%, PS	49
	GITs of fish	NA	NA	50
	Invertebrates	D: H_2O_2, chitinase, protease	90–180 μm, 50.0 ± 4.4%, PE 100–500 μm, 85.3 ± 5.7%, PS 100–500 μm, 81.3 ± 4.2%, PC	44
	Antarctic krill and salps	Modified UEPP	NA	51
	Material from bar screens, influent wastewater, digested sludge, and effluent of a WWTP	D: alcalase, cellulase, Fenton's reagent DS: $ZnCl_2$	NA	52
HYPERION 3000	Samples collected from the air	D: Fenton's reagent, protease, cellulase, chitinase DS: $ZnCl_2$	NA	53
	Drinking water treatment plant treated water	NA	NA	54
	River/lake water	D: H_2O_2 DS: $ZnCl_2$	NA	54
	Estuary water	Modified UEPP	NA	55
	Effluent of WWTPs	Modified UEPP	NA	56
	Mussel	Modified UEPP	NA	57
	Sediment	D: Fenton's reagent DS: $ZnCl_2$	NA	58
	Zooplankton	D: H_2O_2 or HNO_3 DS: NaCl	15 μm, 54%, PS	59

Table 2 (*Contd.*)

IR instrument	Sample types	Pretreatment[b]	Size, % recovery, and particle type	Reference
LUMOS II	Ground water	D: H_2O_2 DS: LMT		60
	Clam	D: KOH DS: $ZnCl_2$	NA	61
	Soil	DS: CsCl	140–954 μm, 94–99%, PA 128–1636 μm, 86–98%, PET	62
	Soil	D: H_2O_2 DS: $ZnCl_2$	NA	9
	Pristine MPs	NA	NA	9
	Corn flour	NA	NA	26
8700 LDIR	Samples collected from the air	D: HNO_3	NA	63
	Atmospheric dustfall	D: H_2O_2 DS: $ZnCl_2$	NA	64
	Indoor house dust	NA	NA	65
	Gel tape	D: glacial acetic acid, H_2O_2 DS: NaI	NA	66
	Bottled water and air deposition	NA	NA	67
	Bottled water	NA	NA	68 and 69
	Groundwater	D: H_2O_2 DS: $ZnCl_2$	NA	70
	Groundwater	D: H_2O_2 DS: $CaCl_2$	75–90 μm, 70%, PE 250–300 μm, 68%, PE	71
	Water from reservoir, dune filtrate, riverbank, and groundwater	D: KOH, H_2O_2 DS: $ZnCl_2$	100 μm, 65–80%, PE	72
	Surface water, groundwater, and water from different stages of drinking water treatment	D: KOH, H_2O_2 DS: $ZnCl_2$	NA	73
	Surface water of a river	D: H_2O_2 DS: $ZnCl_2$	NA	74
	Surface water of a river	D: H_2O_2 DS: NaCl	100–200 μm, 96 ± 2.83%, PE	75
	Surface water of a river	D: H_2O_2	NA	76
	Surface water of a river	D: Fenton's reagent	125–250 μm, 88.3 ± 1.2%	77
	Surface water and bottom water of a river	D: Fenton's reagent DS: $ZnCl_2$	96%, PE; 94%, PP; 96%, PS 92%, PP–PE copolymer 90%, PVC; 94%, PET	78
	Fjord water	D: Fenton's reagent DS: NaCl	NA	79
	Influents and effluents from WWTPs	D: H_2O_2 DS: $ZnCl_2$	NA	80
	Effluents from a WWTP	D: H_2O_2 DS: $ZnCl_2$	100 μm, 90%, PE	81
	Influent and effluent of a petrochemical WWTP	D: H_2O_2 DS: $ZnCl_2$	90.0%, PE; 76.0%, PP 90.9%, resin; 100%, PU 85.4%, PVC; 87.0%, CPE	82

Table 2 (*Contd.*)

IR instrument	Sample types	Pretreatment[b]	Size, % recovery, and particle type	Reference
	Sea water	D: HNO_3 DS: NaCl	200–500 μm, 115 ± 30%, PP 83 ± 10%, PE; 100 ± 15%, PS 148 ± 49%, PVC; 115 ± 35%, PET	83
	Sea water	D: proteinase, H_2O_2, Fenton's reagent, chitinase (the D was microwave-assisted) DS: $ZnCl_2$	20–63 μm, 98.3 ± 0.3%, PET 95 ± 4%, HDPE	84
	Sand	DS: NaCl	20–160 μm, 98%, PP	85
	Sediment	D: H_2O_2 DS: $ZnCl_2$	NA	76
	Sediment	DS: NaCl	200–500 μm, 93 ± 4%, PP 98 ± 17%, PE; 107 ± 43%, PS 153 ± 65%, PVC; 93 ± 20%, PET	83
	Sediment and scum of a septic tank	D: Fenton's reagent, HNO_3 DS: NaCl, NaI	NA	86
	Soil	D: H_2O_2 DS: $ZnCl_2$	NA	9 and 63
	Soil	D: Fenton's reagent, H_2O_2 DS: NaCl, NaI	100 μm, 83.9 ± 5.5%, PVC 0.5–5 mm, 91.1 ± 6.7%, PE	87
	Soil	D: H_2O_2 DS: NaCl	NA	88
	Sludge of a petrochemical WWTP	D: Fenton's reagent, H_2O_2 DS: $ZnCl_2$	87.6%, PE; 78.3%, PP 88.7%, resin; 95.3%, PU 83.2%, PVC; 88.6%, CPE	82
	Mineralized refuse and leachate samples of a landfill	D: H_2O_2 DS: $ZnCl_2$	95.8 ± 3.5%, PET; 88.3 ± 4.7%, PC; 95.5% ± 0.7%, PP; 97.0 ± 1.4%, PE	89
	GITs of fish	D: KOH, H_2O_2	200–300 μm, 88 ± 4%, PS, PP, PVC, PET, PE; 1–5 mm, 76 ± 7%, PET fibre	90
	Mussel	D: HNO_3 DS: NaCl	200–500 μm, 69 ± 17%, PP 78 ± 7%, PE; 101 ± 9%, PS 143 ± 35%, PVC; 81 ± 22%, PET	83
	Snail	D: KOH, H_2O_2 DS: NaCl	100–200 μm, 90 ± 1.25%, PE	75
	Human intestinal and nasal secretions	D: HNO_3	NA	63
	Human intestinal and nasal secretions	NA	NA	91
	Human placenta	D: KOH	50–210 μm and 60–330 μm 88.00 ± 10.58%	92
	Human placentas, meconium, infant feces, breast milk and infant formula	D: HNO_3	96%, PP; 97%, PE; 96%, PS 91%, PET; 87%, PVC; 84%, PU	93
	Human respiratory tract	D: HNO_3	92%, PS; 89%, PP; 78%, PE	94
	Human sputum	D: HNO_3, NaOH DS: $ZnCl_2$	<333 μm, 96%, PP; 97%, PE 96%, PS; 91%, PET; 93%, rubber 87%, PVC; 84%, PU; 6%, PA	95

Table 2 (*Contd.*)

IR instrument	Sample types	Pretreatment[b]	Size, % recovery, and particle type	Reference
SPERO microscope	Treated wastewater, marine surface water, marine sediment, snow samples, pristine MPs	NA	NA	11
mIRage microscope	Baby teat	NA	NA	13
	Corn flour	NA	NA	26
	Sea water	MP concentrator	>90%	96
	Plastic food container	MP concentrator	>90%	96
	Deep-sea sediment	DS: NaCl MP concentrator	>90%	96
	Fish tissue spiked with MPs	D: HNO_3, H_2O_2	<60 μm, 87–97% 60–100 μm, 87–100% 100–200 μm, 87–107% 200–500 μm, 90–110%	97
mIRage+R microscope	Soil	D: H_2O_2 DS: $ZnCl_2$	NA	9
	Pristine MPs	NA	NA	9
Nano IR2	Masterbatches (composed of pigment red and LDPE)	NA	NA	98
	PP film (largest dimension <5 mm)	NA	NA	12
	TiO_2 coated PP particles	NA	NA	99

[a] MP = microplastic, WWTP = wastewater treatment plant, GIT = gastrointestinal tract, $ZnCl_2$ = zinc chloride, SPT = sodium polytungstate, NaCl = sodium chloride, H_2O_2 = hydrogen peroxide, LMT = lithium metatungstate, LST = lithium heteropolytungstate, KOH = potassium hydroxide, NaOH = sodium hydroxide, CsCl = caesium chloride, HNO_3 = nitric acid, NaI = sodium iodide, $CaCl_2$ = calcium chloride, TIO_2 = titanium dioxide, PP = polypropylene, PS = polystyrene, PE = polyethylene, PC = polycarbonate, PET = polyethylene terephthalate, PU = polyurethane, PVC = polyvinyl chloride, PA = polyamide (nylon), CPE = chlorinated polyethylene, LDPE = low density polyethylene, HDPE = high density polyethylene, UEPP = Universal Enzymatic Purification Protocol. [b] D = digestion, DS = density separation.

organic materials. Compared to the widely used MNP extraction methods based on Fenton's reagent or enzymes (Table 2), the Co/PMS system is much less dependent on pH or temperature, and can remove organic matter in a much shorter time.[101] Specifically, to effectively remove organic matter from a MNP sample using Fenton's reagent or enzymes, the operating temperature and pH need to be adjusted to the range where Fenton's reagent or enzymes work best, and, even under optimal conditions, the removal process generally takes one to several days. In contrast, the Co/PMS system can rapidly (<1 h) remove organic matter from a MNP sample at room temperature and can do it within a wide pH range (2–8). Other advantages of the Co/PMS system include that it does not damage MNPs or cause particle losses, it does not alter the physical or chemical properties of MNPs, and *etc.* It can be expected that the Co/PMS system will be adopted by more studies and institutions for MNP extraction/purification in future due to its advantages, meeting the need for routine monitoring of MNPs.

In a study using near-field molecular spectral imaging to detect MPs in corn flour, the corn flour was intentionally spiked with MPs and the MPs were not subsequently extracted.[26] This is because the primary research objective of this study was to directly detect MPs in corn flour. To explore the self-assembly of extracellular polymeric substances (EPS) on the surface of MPs, MPs were deliberately immersed in an EPS solution and then were lyophilised.[12] To study the changes in the microstructure of the MP surface, the MPs were artificially oxidised,[98] or coated.[99]

As the last step before IR spectroscopic analysis, the extracted or intentionally treated MNPs or samples spiked with MNPs were typically deposited on or transferred to a substrate.

For FTIR microscopes, the working mode (*i.e.*, transmission, reflection/transflectance) decides the type of substrates/filters needed. In transmission mode, IR radiation that passes through the sample is detected. Therefore, IR-transparent/weak-IR-absorbent substrates/filters are required for this mode. Commonly used IR-transparent/weak-IR-absorbent substrates/filters include zinc selenide windows, aluminium oxide filters, polycarbonate filters, calcium fluoride windows, and barium fluoride windows. In reflection mode, the IR beam that passes through the sample, reflects off a substrate/filter, and travels back through the sample a second time is measured. Hence, IR-refractive substrates/filters are required. Examples of IR-refractive substrates/filters include the MirrIR Low-E slides, silver membranes, and gold-coated filters.

For the SPERO microscope, the choice of substrate/filter also depends on whether the transmission or reflection mode is employed. In transmission mode, IR transparent substrates/filters are required, while in reflection mode, IR reflective substrates/filters are needed. In the only identified article that used the SPERO microscope for MP analysis, the researchers analysed MPs placed on barium fluoride windows and on aluminium oxide filters (placed on barium fluoride windows) in transmission mode.[11] The 8700 LDIR typical works in transflectance mode for MP analysis and only accepts IR reflective glass slides for loading samples. Among the 34 publications that utilised the 8700 LDIR, 11 of them used Kevley/MirrIR IR reflective slides, and 16 used highly refractive slides (although the slide manufacturer was not explicitly specified), while the remaining publications did not specify what slides were used. For those users of the 8700 LDIR using filters to concentrate MPs, they needed to transfer the MPs from the filters to IR refractive glass slides. To achieve this, the filter containing MPs was shaken and sonicated in an ethanol solution to dislodge the MPs. The ethanol solution was then concentrated and dripped onto the slide. After the ethanol evaporated, the MPs on the glass slide were ready for analysis. However, the practice of transferring MPs from filters to IR reflective slides has faced criticism as it might cause particle loss/aggregation. As an alternative, the direct placement of an IR transparent filter containing MPs onto an IR reflective slide has been proposed.[83]

Rather than measuring residual IR radiation, O-PTIR microscopes measure the sample's intrinsic IR absorption by monitoring changes in the intensity of the visible laser probe. In principle, in the reflection mode, as long as the visible light (the probe) can escape from the sample surface and reach the detector, O-PTIR spectra can be obtained. This process is not significantly influenced by the IR transmissivity or reflectivity of the substrate/filter. Therefore, both IR transparent and IR reflective substrate/filters have been used in MNP studies employing O-PTIR microscopes (in the reflection mode). It is noteworthy that the mIRage microscope operates in reflection mode only, while the mIRage+R microscope can work in transmission mode, where the intensity of the transmitted probe beam is monitored. Currently, the transmission mode of the mIRage+R microscope has not been used in MNP research. Suitable substrates/filters for the transmission mode should allow the probe beam to pass through without altering its intensity. A calcium fluoride window is one of the suitable substrates for transmission O-PTIR spectroscopy;[103] however, transferring MPs from filters remains problematic.

An ideal substrate/filter for the AFM-IR technique to detect MNPs should meet the criteria of both AFM and IR: the surface of the substrate/filter should be smooth, and the IR background should be low. Additionally, substrate metallisation has been suggested to play a role in improving the quality of AFM-IR spectra.[104] These features of a substrate/filter have a significant impact on the analysis of thin objects; however, their effects would be minimised when analysing relatively thick (>500 nm) objects.[105] Among the three studies that used the AFM-IR technique for MNP analysis, Xu *et al.*[12] investigated a 3 mm × 3 mm plastic film, but the thickness of the film and the type of substrate used were not reported; Luo *et al.*[98] studied MPs captured on a filter with a pore size of 0.45 μm, but the filter type was not specified; in another study by Luo *et al.*,[99] plastic films with an equivalent diameter of 3–5 mm and a thickness of about 1 mm were analysed using a silicon wafer as the substrate. However, the effects of substrates/filters were not reported in any of these studies.

3.1.3. Data quality. The spectral range and quality play a crucial role in MNP analysis. Insufficient range and/or poor spectral quality can lead to incorrect identification results, such as misidentifying non-MNPs as MNPs. The results summarised in this review indicate that the commonly used spectral ranges

for the FPA-FTIR instruments are as follows: 3800–800 cm^{-1} for the Cary 620, 3600–1250 cm^{-1} for the HYPERION 3000 and 4000–800 cm^{-1} for the LUMOS II. These ranges cover both the IR functional group region and the fingerprint region. In contrast, the SPERO microscope and the 8700 LDIR have a limited spectral range of around 1800–800 cm^{-1}, covering the full fingerprint region and part of the functional group region. The O-PTIR microscopes also have a spectral range of ~1800 to 800 cm^{-1}, owing to the use of a standard QCL (however, the spectral range of the O-PTIR microscopes could be extended, as discussed in Section 1.1.3). The Nano IR2 covers a spectral range of ~3600 to ~900 cm^{-1}.

Spectral resolution is an important metric for evaluating spectral quality and refers to the ability of an IR instrument to distinguish between bands that are in close proximity. Typically, the spectral resolution can be set to values such as 16 cm^{-1}, 8 cm^{-1}, 4 cm^{-1}, or 2 cm^{-1}. Generally, a higher spectral resolution allows for better representation of small IR bands. However, acquiring high-resolution spectra may lead to longer data acquisition time and larger file sizes. Studies have suggested that a resolution of 8 cm^{-1} is optimal for MP research using FTIR spectroscopy,[106] as it provides the best balance between spectral quality and data acquisition time. Engaging in instrument comparison based on the spectral resolution of spectra generated by different instruments is not applicable. This is because spectral resolution is typically user-defined rather than an inherent instrument attribute.

SNR is also an important metric for evaluating spectral quality. High SNR spectra have clear signals and are easier to interpret. Increasing the number of co-added scans (*e.g.*, 6 scans) has been reported to significantly improve the SNR of the spectrum,[106] but this also increases the data collection time. Under equivalent scan numbers, instruments equipped with QCLs exhibit higher SNR compared to the FTIR microscopes. This advantage can be attributed to the inherent high photon flux of QCLs.[18] For users of O-PTIR microscopes, the improvement of SNR can be achieved not only by increasing the number of co-added scans but also by elevating the power of the pump (IR) laser and/or the power of the probe laser. However, it is important to be careful when increasing the power of the lasers, as excessive power levels may risk damaging the sample. The SNR of the Nano IR2, which employs an OPO laser as the IR source, is comparatively subdued due to the low repetition rate of the OPO laser.[25]

The presence of spectral artefacts has been considered a key indicator for evaluating the quality of spectra. When investigating minute substances such as MP particles using the FTIR or QCL-IR technique, the acquired spectra often encompass a diverse range of spectral artefacts. Among these, the most prominent and challenging artefact is the so-called dispersion artefact, primarily associated with resonant Mie scattering.[107] This dispersion artefact arises when the size of the sample is comparable to the wavelength of the incident IR light. It compromises the quality of spectra and has two main manifestations: firstly, it results in a broad sinusoidal oscillation in the spectrum's baseline, leading to distortions in both the position and intensity of absorption bands. Secondly, it induces considerable distortions in the shape of spectral bands, notably a derivative-like distortion on the high-wavenumber side of the amide I band. To mitigate the impact of resonant Mie scattering or dispersion artefact, several computational algorithms have been proposed.[107,108] Other notable spectral artefacts associated with FTIR spectroscopy or QCL-IR spectroscopy include artefacts arising from the morphology of the sample. Briefly, when analysing samples with rough surfaces in transflectance mode, strong light scattering (due to the rough surface) would occur and disrupt the reflected signal, ultimately resulting in compromised spectra.

The fundamental cause of these spectral artefacts is the measurement of residual IR radiation by FTIR and QCL-IR instruments, and the residual IR radiation can be interfered with by phenomena such as resonant Mie scattering. On the contrary, the O-PTIR technique and the AFM-IR technique do not measure residual IR radiation, making them immune to such spectral artefacts. Fig. 6 presents an O-PTIR spectrum and a SPERO transmission spectrum (*i.e.*, one collected using the SPERO microscope in transmission mode) of a 10 μm nylon particle. It can be seen that the SPERO spectrum exhibits traces of dispersion artefact, indicated by the presence of a first derivative-like line shape in the vicinity of the carbonyl stretching mode (as indicated by the black arrow in the figure). Additionally, a subtle oscillation of the baseline is discernible. In contrast, the region of the carbonyl stretching mode in the O-PTIR spectrum remains unaffected, and the baseline of the spectrum appears comparatively flat, indicating the immunity of the O-PTIR technique against dispersion artefact.

3.1.4. Spatial resolution and detection limit. Currently, there is a requirement to analyse smaller MNPs, in which the spatial detection limit of the instrument becomes particularly important. The lower the spatial detection limit of an instrument, the more reliable results it can provide for analysing tiny MNP particles. Generally, the spatial detection limit of an

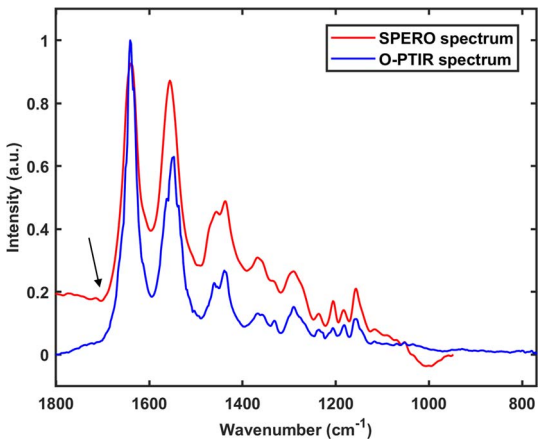

Fig. 6 A spectrum of a 10 μm nylon particle obtained using the SPERO microscope in transmission mode and an O-PTIR spectrum of another 10 μm nylon particle. The spectral range of the SPERO spectrum is 1900–948 cm^{-1}. The spectral range of the O-PTIR spectrum is 1801–769 cm^{-1}. The black arrow indicates where a first derivative-like line shape could be seen in the SPERO spectrum.

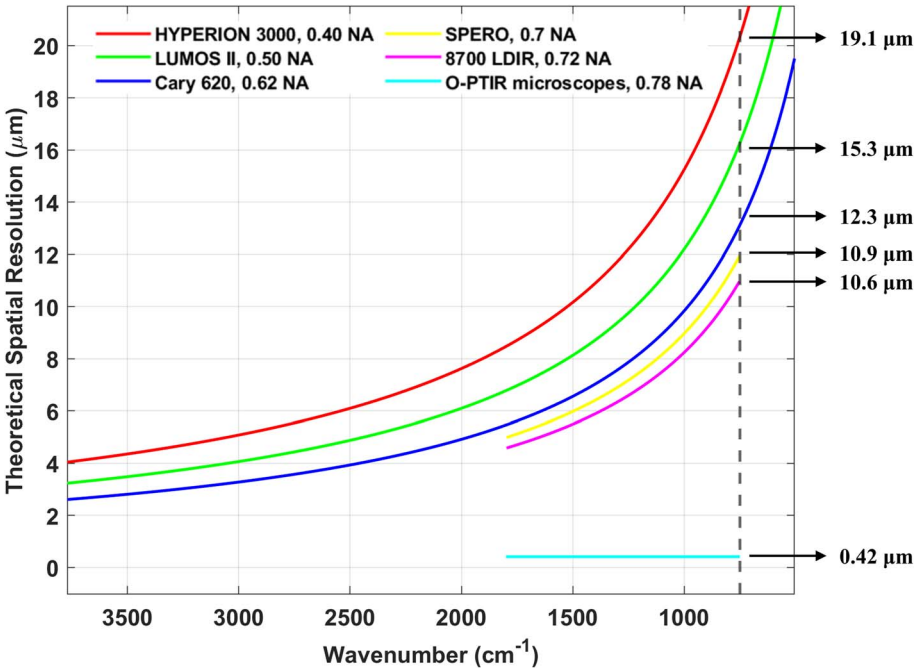

Fig. 7 The theoretical spatial resolution of the instruments compared in this review (excluding the Nano IR2). For instruments that use a QCL as the IR source, the spatial resolution curve is limited to the typical working range of the QCL (~1800 to ~800 cm^{-1}). The vertical black dashed line and arrows in the graph indicate the theoretical spatial resolution of each instrument at 800 cm^{-1}.

instrument is closely related to its theoretical spatial resolution, the higher the theoretical spatial resolution, the lower the spatial detection limit. Fig. 7 displays the spatial resolution of the IR instruments compared in this review (except for the Nano IR2), based on the Rayleigh criterion (theoretical spatial resolution = 0.61λ/NA, where λ is the wavelength of the IR light of FTIR or QCL-IR instruments, or the wavelength of the probe laser of O-PTIR microscopes, NA is the numerical aperture). The vertical dashed line in the figure indicates the theoretical spatial resolutions of the compared instruments at 800 cm^{-1}. It can be observed that the FTIR and QCL-IR instruments have similar spatial resolutions, and both change with the IR wavelength. The resolution of the O-PTIR microscopes is determined by the wavelength of the probe laser and remains constant at 0.42 µm (when a 532 nm probe laser is used). The Nano IR2's spatial resolution is influenced by the size of its probe tip, generally around 20 nm. It is worth noting that for FPA-FTIR, if the projected pixel size of the FPA is larger than the theoretical spatial resolution (*e.g.*, due to binning by the user), the projected pixel size, rather than the wavenumber of light, becomes the limiting factor for spatial resolution and subsequently, the spatial detection limit.

Based on our findings, the reported detection limit for FPA-FTIR is typically in the range of 10 to 20 µm. For FPA detectors with a projected pixel size smaller than the detection limit, "particles" smaller than the detection limit (*i.e.*, particles occupying only one pixel) might be detected. Nevertheless, such "particles" should be treated with caution or excluded from the analysis since they could be false positives. To address this issue, binning is commonly employed by FPA-FTIR users to increase the pixel size to a value greater than the diffraction limit, effectively eliminating these false positives. With the 8700 LDIR, users can set the detection limit themselves. Most users set the detection limit at 20 µm, while a minority set it at 10 µm. The official documentation for the 8700 LDIR states that analysing MPs larger than 20 µm tends to yield relatively reliable results, while the reliability decreases for MPs in the 10 to 20 µm range. However, a recent study has shown that the 8700 LDIR might miss or overlook particles smaller than 60 µm.[9] Regarding the SPERO microscope, Primpke *et al.*[11] reported detection of MPs with a size of 4.2 µm (at low magnification) and 1.4 µm (at high magnification), which corresponds to the projected sizes of the FPA detector of the SPERO microscope. However, it is important to note that such small-sized MPs should not be considered reliable results unless tested against binned measurements.[11] This is because the fundamental detection limit of the SPERO microscope is 10.9 µm (Fig. 7) due to the diffraction limit of light. In studies using the O-PTIR microscopes, the smallest detected MNP particle size was reported to be 600 nm,[13] suggesting that the detection limit of the mIRage/mIRage+R microscope with a 532 nm probe laser is at least 600 nm. As for the Nano IR2, though the theoretical detection limit can reach around 20 nm, the actual detection limit was not explored in the studies covered in this review, as the focus of these studies was on the surface/physical characteristics of relatively large MNPs.

3.1.5. Data acquisition speed. For the routine monitoring of environmental MNPs, instruments with fast data acquisition speeds are advantageous. When comparing the data acquisition speeds of different instruments, it is essential to consider the

time taken to acquire a single spectrum and imaging speed. However, the time taken to acquire a single spectrum is rarely reported. Scattered pieces of evidence suggest that the 8700 LDIR takes approximately 6–9 seconds to analyse a single particle.[9] Our in-house mIRage O-PTIR microscope takes 15 seconds to acquire a spectrum from a single particle (3 scans). The speed of collecting spectra from individual particles using the FPA-FTIR instruments is not available in the published work covered in this review. However, it is well-documented that instruments that use QCLs as the light source have a significantly faster data collection rate compared to (FPA-)FTIR instruments,[11] even up to 150 times faster at an equivalent SNR.[18] The speed for the Nano IR2 to collect a spectrum is not available in the articles evaluated in this review.

Imaging speed is defined here as the time required to perform hyperspectral imaging on a certain area. The imaging speed of instruments equipped with an FPA detector primarily depends on factors such as spatial resolution, FPA size (*e.g.*, 32 × 32, 64 × 64, 128 × 128), number of scans, and the IR source used. The SPERO microscope benefits from having a large FPA detector (480 × 480) and a QCL, making it the fastest in terms of imaging. It has been reported that the SPERO microscope could image a 144 mm^2 area in just 36 minutes with a pixel resolution of 4.2 μm.[11] The imaging speeds of the Cary 620 and HYPERION 3000 are slower than the SPERO microscope because they use thermal Globar as the IR radiation source, and their FPA size is only 64 × 64. Following them is the LUMOS II, which has an FPA size of 32 × 32. Dong *et al.*[9] reported that the LUMOS II achieved an imaging speed of 9 minutes per mm^2 (spectral resolution of 8 cm^{-1}, no binning, 2 scans). For instruments without an FPA detector, imaging relies on a single-element detector and a motorised stage, resulting in significantly slow speeds. For example, our in-house mIRage O-PTIR microscope requires approximately two full weeks to perform hyperspectral imaging on a 480 μm × 640 μm area (spectral range: 1801–769 cm^{-1}, spectral resolution: 2 cm^{-1}, spatial resolution: 2 μm, number of scans: 5).

3.1.6. Data processing. Depending on the method used to analyse MNPs, IR instruments usually produce two types of data: hyperspectral data and point spectra. Typically, the processing of hyperspectral data includes three main steps: (1) spectral preprocessing, which aims to reduce instrumental artefacts or differences caused by factors unrelated to the sample's chemical composition. Chemometric methods such as multiplicative scatter correction (MSC) and standard normal variate (SNV) are commonly used for this purpose. (2) Pixel classification, which is performed to classify the unknown spectra in the hyperspectral data for identification purposes. This can be achieved through instance-based or model-based machine learning approaches. (3) Image analysis, which is used to obtain information about the size, shape, and quantity of MNP particles. Software tools such as siMPle[109] and Purency Microplastics Finder[28] have been developed specifically for processing hyperspectral data of MPs, and these tools have been widely adopted by researchers in the field. As for the collected point spectra, it is common to directly perform a library search for identification (or apply preprocessing steps such as smoothing and baseline removal before performing a library search).

Our findings reveal that over half of the FPA-FTIR users used the software siMPle (available for free at **https://simple-plastics.eu/**) for processing hyperspectral data and polymer identification. siMPle is software designed for automated MP analysis and it is an instance-based machine learning approach.[27] This software uses Pearson's correlation coefficient as a metric to gauge the degree of correlation between each sample spectrum and reference spectra. Importantly, there exist three distinct Pearson's correlation coefficients, to which the user assigns global weights (weight raw/weight 1st/weight 2nd). In addition, siMPle is capable of providing information concerning the size of particles. Users could not only fine-tune the global weights to suit their needs but also set thresholds for the identification of particles. Furthermore, the software affords users the flexibility to incorporate external reference spectra into the built-in spectral library. FPA-FTIR users who did not use siMPle for data analysis employed alternative software tools such as ImageLab (Epina GmbH, Austria) in conjunction with a non-commercial, custom-made software tool based on random forest decision classifiers,[53,57,62] or Purency Microplastics Finder.[9] A few users did not provide detailed descriptions of how they processed the hyperspectral data. The hyperspectral data generated by the SPERO microscope was processed using a custom-written Python script.[11]

The 8700 LDIR mainly collects point spectra. Users of the 8700 LDIR typically employed the Clarity software (Agilent) for MP identification and characterisation. Clarity is a software tool tied to the 8700 LDIR, and it has an automated particle analysis workflow specifically tailored for MP analysis. In this workflow, a single frequency chemical image at 1800 cm^{-1} is initially generated, and Clarity counts and measures these particles. Subsequently, the spectra of all particles in this chemical image are obtained and compared to the spectral library automatically. For the library search, Clarity utilises derivative spectral treatment. The software comes with a built-in polymer reference library, and users have the option to import external reference spectra.

Unlike FPA-FTIR or 8700 LDIR users, O-PTIR microscope users do not follow a fixed data processing approach. For point spectra collected by O-PTIR microscopes, users might choose to perform Savitzky–Golay smoothing using the software PTIR studio (Photothermal Spectroscopy Corp)[96] before comparing the spectra with spectral libraries for identification purposes. Hyperspectral data acquired using an O-PTIR microscope was processed using an in-house script, which included SNV, correlation coefficient calculation, and independent component analysis, to visualise the distribution of MPs within the sample matrix.[26]

Users of the Nano IR2 collected point spectra and single frequency images of MPs before and after treatment to elucidate the alterations in the nanoscale IR, thermal, and mechanical properties of the MPs analysed. This process solely involved examining the changes in spectra and single frequency images before and after treatment. Therefore, only basic data processing such as Savitzky–Golay smoothing might be employed.[98]

Table 3 Summary of the comparison of IR instruments in terms of their spectral range, spectral quality, imaging speed, theoretical detection limit, size of the smallest MNP detected and cost

Technique	Instrument	Spectral range[a]	Spectral quality	Imaging speed[c]	Theoretical detection limit	Size of the smallest MNP detected[f]	Cost
FPA-FTIR	Cary 620	Broad	Low SNR, susceptible to spectral artefacts	Fast	12.3 μm	10–20 μm	∼$300k
	HYPERION 3000	Broad	Low SNR, susceptible to spectral artefacts	Fast	19.1 μm	10–20 μm	∼$350k
	LUMOS II	Broad	Low SNR, susceptible to spectral artefacts	Fast	15.3 μm	10–20 μm	∼$200k
QCL-IR	SPERO microscope	Narrow	High SNR, susceptible to spectral artefacts	Very fast	10.9 μm	1.4 μm	∼$500k
	8700 LDIR	Narrow	High SNR, susceptible to spectral artefacts	Slow	10.6 μm	10–20 μm	∼$350k
O-PTIR	mIRage microscope	Narrow[b]	High SNR, immune to spectral artefacts	Slow	0.42 μm[d]	0.6 μm	∼$500k
	mIRage+R microscope	Narrow[b]	High SNR, immune to spectral artefacts	Slow	0.42 μm[d]	∼0.6 μm	∼$600k
AFM-IR	Nano IR2	Broad	Low SNR, immune to spectral artefacts	Slow	∼20 nm[e]	NA	NA

[a] "Broad" represents a spectral range of ∼3800 cm^{-1} to ∼900 cm^{-1}, while "Narrow" represents a range of ∼1800 cm^{-1} to ∼800 cm^{-1}. [b] The spectral range of an O-PTIR microscope could be extended by either changing the IR source or adding an additional IR source. [c] Imaging speed is the speed of hyperspectral imaging. [d] The theoretical detection limit depends on the wavelength of the probe. 0.42 μm corresponds to the use of a 532 nm probe. [e] The theoretical detection limit depends on the size of the probe tip and is roughly the size of the probe tip. [f] Including environmental MNPs, and these results are based on the studies covered in this review.

3.1.7. Cost. When comparing different instruments, an essential parameter that demands careful consideration is the cost. However, cost is not available in all the studies covered in this review. After consulting additional sources, limited information was found, which revealed that the Cary 620, the HYPERION 3000, the LUMOS II, and the 8700 LDIR fall within a similar price range, all priced below 500k USD. Conversely, the SPERO microscope, the O-PTIR microscopes, and the Nano IR2 are associated with considerably higher prices.

The results of the comparison of the IR instruments conducted in this section are summarised in Table 3. In MNP analysis, the distinctive merits of the Cary 620, the HYPERION 3000, and the LUMOS II lie in their ability to accommodate an FPA detector, coupled with their cost-effectiveness, albeit with constraints in spectral quality (low SNR and susceptible to spectral artefacts) and analysis of smaller MPs or NPs. The SPERO microscope shines in its exceptional imaging speed, yet it is associated with a higher price tag, a limited spectral range, and compromises in imaging quality (for details see Section 4). A standout feature of the 8700 LDIR is its intelligent software Clarity, which empowers rapid and automated analysis of MPs. Nonetheless, it is important to note its narrow spectral range, and concerns have arisen regarding the accuracy of this instrument when it is used to analyse MPs smaller than 60 μm.[9] The notable feature of the O-PTIR microscopes is the capability to analyse MNP sized down to around 0.5 μm. However, it is essential to recognise that these microscopes are paired with a single-element detector, resulting in a sluggish imaging speed, and they belong to a higher price range. The Nano IR2 can provide a nano-level imaging resolution. Nevertheless, its SNR is low and imaging speed is limited.

4. Challenges and recommendations

The monitoring of MNPs in environmental contexts, water supplies, and food safety holds significant importance for both consumers and governments.[11] Initially, the analysis of MNPs was inaccurate and labour-intensive. However, with advancements in IR instruments (as well as in other kinds of instruments such as Raman microscopes), MNP analysis has been made easier and even automated. FPA-FTIR microscopes, the SPERO microscope, and the 8700 LDIR are effective in the automated analysis of MPs, with the SPERO microscope and the 8700 LDIR being faster than FPA-FTIR microscopes. Nevertheless, these instruments are affected by the diffraction of light, which means they cannot reliably analyse MPs smaller than 20 μm or 10 μm. To address this challenge, increasing the NA of the IR objective is one approach.

Undoubtedly, using a QCL as the IR source, and being equipped with a large FPA detector, the SPERO microscope is super-fast in imaging MP samples. However, it is essential to recognise that the high degree of coherence of the QCL can unavoidably lead to severe image distortions, such as fringes and speckles,[20] hindering a meaningful interpretation of hyperspectral images and thereby affecting the reliable analysis of MPs. To mitigate the impact of spatial coherence phenomena, Schönhals *et al.*[20] proposed the use of both a moving and a stationary scatterer/diffuser to reduce the time-averaged spatiotemporal coherence properties of the illumination.

An additional challenge concerning the image quality of the SPERO microscope pertains to the noticeable artefacts at the junctions of hyperspectral tiles, as illustrated in Fig. 8. This

Fig. 8 Hyperspectral images composed of hyperspectral tiles that were collected using our in-house SPERO microscope. The image reveals a lack of harmony at the junction where the two hyperspectral tiles are joined. The horizontal midline of the images marks the location where the hyperspectral tiles meet.

figure is composed of the upper hyperspectral tile and the lower hyperspectral tile, and the horizontal midline of the image is where the two tiles meet. It can be seen that the upper hyperspectral tile and the lower hyperspectral tile are not aligned correctly. This misalignment may be attributed to inaccuracies in the motorised stage. This issue can be addressed by manually adjusting the relative positions of the hyperspectral tiles or by fine-tuning the motorised stage. Additionally, from Fig. 8, it is evident that the brightness of the lower edge of the upper hyperspectral tile and the upper edge of the lower hyperspectral tile is inconsistent. The underlying cause of this occurrence could be attributed to the uneven illumination of the FPA, resulting in inconsistent spectral sensitivity across the entire FPA. To rectify this artefact, it is imperative to ensure homogeneous illumination across the FPA.

The O-PTIR microscopes provide submicron-level resolution in the analysis of MNPs, enabling the identification and characterisation of smaller plastic particles. However, their potential for automated analysis of MNPs is limited. Future improvements could involve designing software for the O-PTIR microscopes similar to Clarity.[9] Another opportunity for improvement is the development of a large FPA detector for the O-PTIR microscopes.

5. Conclusion

The globally widespread distribution of MNPs is well-documented, encompassing their presence in the air, oceans, organisms, flora, and even within the human body. To comprehensively assess the hazards posed by these emerging pollutants, reliable analytical tools are essential. FTIR spectroscopy, QCL-IR spectroscopy, O-PTIR spectroscopy, and AFM-IR spectroscopy are such reliable analytical tools that can provide precise identification and characterisation of MNP particles. The principles of these IR spectroscopic techniques, the advantages, and disadvantages of relevant instruments in MNP analysis, and recommendations for addressing the limitations of some instruments have been discussed in this review article.

It is imperative to acknowledge that the summation of the most advanced IR instruments presented in this review is predicated upon studies published between 2021 and 2023. This snapshot may not holistically encapsulate the latest advancements in the field, as some cutting-edge IR instruments might not have been featured in studies during this specific timeframe.

By gaining an in-depth understanding of the underlying principles of various IR spectroscopic techniques expounded in this review and delineating the merits and limitations of instruments based on these techniques, researchers and practitioners can derive invaluable insights to guide their selection or procurement of IR instruments for MNP research.

Conflicts of interest

There are no conflicts to declare.

Acknowledgements

Funding for this research was provided by the Science Foundation Ireland (SFI)-Irish Research Council Pathway Programme Proposal ID 21/PATH-S/9290.

References

1 L. R. Arenas, S. R. Gentile, S. Zimmermann and S. Stoll, *Sci. Total Environ.*, 2021, **791**, 148175.
2 L. P. Domínguez-Jaimes, E. I. Cedillo-González, E. Luévano-Hipólito, J. D. Acuña-Bedoya and J. M. Hernández-López, *J. Hazard. Mater.*, 2021, **413**, 125452.
3 S. Manzo and S. Schiavo, *Sci. Total Environ.*, 2022, **808**, 152105.
4 R. Ullah, M. T.-K. Tsui, A. Chow, H. Chen, C. Williams and A. Ligaba-Osena, *Environ. Monit. Assess.*, 2023, **195**, 252.
5 N. P. Mortensen, T. R. Fennell and L. M. Johnson, *NanoImpact*, 2021, **21**, 100302.
6 H. A. Leslie, M. J. Van Velzen, S. H. Brandsma, A. D. Vethaak, J. J. Garcia-Vallejo and M. H. Lamoree, *Environ. Int.*, 2022, **163**, 107199.
7 Y. Deng, Y. Zhang, B. Lemos and H. Ren, *Sci. Rep.*, 2017, **7**, 46687.
8 A. Faltynkova, G. Johnsen and M. Wagner, *Microplastics and Nanoplastics*, 2021, **1**, 1–19.
9 M. Dong, Z. She, X. Xiong, G. Ouyang and Z. Luo, *Anal. Bioanal. Chem.*, 2022, **414**, 3359–3372.
10 Y. Chen, D. Wen, J. Pei, Y. Fei, D. Ouyang, H. Zhang and Y. Luo, *Current Opinion in Environmental Science & Health*, 2020, **18**, 14–19.
11 S. Primpke, M. Godejohann and G. Gerdts, *Environ. Sci. Technol.*, 2020, **54**, 15893–15903.

12 S. Xu, C. Wang, P. Zhu, D. Zhang and X. Pan, *J. Hazard. Mater.*, 2022, **440**, 129773.
13 Y. Su, X. Hu, H. Tang, K. Lu, H. Li, S. Liu, B. Xing and R. Ji, *Nat. Nanotechnol.*, 2022, **17**, 76–85.
14 G. Renner, T. C. Schmidt and J. Schram, in *Comprehensive Analytical Chemistry*, Elsevier, 2017, vol. 75, pp. 67–118.
15 B. Man Thaiba, T. Sedai, S. Bastakoti, A. Karki, K. C. Anuradha, G. Khadka, S. Acharya, B. Kandel, B. Giri and B. Bhakta Neupane, *Arabian J. Chem.*, 2023, **16**, 104686.
16 J.-L. Xu, K. V. Thomas, Z. Luo and A. A. Gowen, *TrAC, Trends Anal. Chem.*, 2019, **119**, 115629.
17 S. Primpke, C. Lorenz, R. Rascher-Friesenhausen and G. Gerdts, *Anal. Methods*, 2017, **9**, 1499–1511.
18 A. Ogunleke, V. Bobroff, H.-H. Chen, J. Rowlette, M. Delugin, B. Recur, Y. Hwu and C. Petibois, *TrAC, Trends Anal. Chem.*, 2017, **89**, 190–196.
19 C. Krafft, in *Molecular and Laser Spectroscopy*, ed. V. P. Gupta, Elsevier, 2022, pp. 305–336, DOI: **10.1016/B978-0-323-91249-5.00007-7**.
20 A. Schönhals, N. Kröger-Lui, A. Pucci and W. Petrich, *J. Biophot.*, 2018, **11**, e201800015.
21 J. Reffner, *Spectroscopy*, 2018, **33**, 12–17.
22 M. Kansiz, C. Prater, E. Dillon, M. Lo, J. Anderson, C. Marcott, A. Demissie, Y. Chen and G. Kunkel, *Microsc. Today*, 2020, **28**, 26–36.
23 J. S. Böke, J. Popp and C. Krafft, *Sci. Rep.*, 2022, **12**, 18785.
24 J. R. Felts, K. Kjoller, M. Lo, C. B. Prater and W. P. King, *ACS Nano*, 2012, **6**, 8015–8021.
25 A. Dazzi and C. B. Prater, *Chem. Rev.*, 2017, **117**, 5146–5173.
26 Y. Shi, L. Yi, G. Du, X. Hu and Y. Huang, *Sci. Total Environ.*, 2023, **862**, 160714.
27 S. R. Moses, L. Roscher, S. Primpke, B. Hufnagl, M. G. Löder, G. Gerdts and C. Laforsch, *Anal. Bioanal. Chem.*, 2023, 1–13.
28 B. Hufnagl, M. Stibi, H. Martirosyan, U. Wilczek, J. N. Möller, M. G. Löder, C. Laforsch and H. Lohninger, *Environ. Sci. Technol. Lett.*, 2021, **9**, 90–95.
29 L. M. Hernandez, E. G. Xu, H. C. Larsson, R. Tahara, V. B. Maisuria and N. Tufenkji, *Environ. Sci. Technol.*, 2019, **53**, 12300–12310.
30 K. Busse, I. Ebner, H.-U. Humpf, N. Ivleva, A. Kaeppler, B. E. Oßmann and D. Schymanski, *Environ. Sci. Technol.*, 2020, **54**, 14134–14135.
31 N. Rakovitsky, S. Frenk, H. Kon, D. Schwartz, E. Temkin, E. Solter, S. Paikin, R. Cohen, M. J. Schwaber and Y. Carmeli, *J. Clin. Microbiol.*, 2020, **58**(5), e00098.
32 R. Salzer, *Anal. Bioanal. Chem.*, 2008, **391**, 2379–2380.
33 J. A. Reffner, *Microsc. Today*, 1993, **1**, 6–7.
34 E. N. Lewis, P. J. Treado, R. C. Reeder, G. M. Story, A. E. Dowrey, C. Marcott and I. W. Levin, *Anal. Chem.*, 1995, **67**, 3377–3381.
35 S. M. Mintenig, I. Int-Veen, M. G. Löder, S. Primpke and G. Gerdts, *Water Res.*, 2017, **108**, 365–372.
36 L. Feld, V. H. d. Silva, F. Murphy, N. B. Hartmann and J. Strand, *Water*, 2021, **13**, 2097.
37 J. Weisser, I. Beer, B. Hufnagl, T. Hofmann, H. Lohninger, N. P. Ivleva and K. Glas, *Water*, 2021, **13**, 841.
38 I. V. Kirstein, F. Hensel, A. Gomiero, L. Iordachescu, A. Vianello, H. B. Wittgren and J. Vollertsen, *Water Res.*, 2021, **188**, 116519.
39 Y. Liu, C. Lorenz, A. Vianello, K. Syberg, A. H. Nielsen, T. G. Nielsen and J. Vollertsen, *Sci. Total Environ.*, 2023, **865**, 161255.
40 A. F. dos Santos Queiroz, A. S. da Conceição, D. Chelazzi, M. Rollnic, A. Cincinelli, T. Giarrizzo and J. E. Martinelli Filho, *Sci. Total Environ.*, 2022, **839**, 156259.
41 E. Uurasjärvi, M. Pääkkönen, O. Setälä, A. Koistinen and M. Lehtiniemi, *Environ. Pollut.*, 2021, **268**, 115700.
42 K. Gunaalan, R. Almeda, C. Lorenz, A. Vianello, L. Iordachescu, K. Papacharalampos, C. M. R. Kiær, J. Vollertsen and T. G. Nielsen, *Environ. Pollut.*, 2023, **318**, 120853.
43 C. Scopetani, D. Chelazzi, T. Martellini, J. Pellinen, A. Ugolini, C. Sarti and A. Cincinelli, *Mar. Pollut. Bull.*, 2021, **171**, 112712.
44 C.-G. Pan, S. M. Mintenig, P. E. Redondo-Hasselerharm, P. H. Neijenhuis, K.-F. Yu, Y.-H. Wang and A. A. Koelmans, *Environ. Sci. Technol.*, 2021, **55**, 9916–9925.
45 S. Saarni, S. Hartikainen, S. Meronen, E. Uurasjärvi, M. Kalliokoski and A. Koistinen, *Environ. Pollut.*, 2021, **274**, 116568.
46 A. Cincinelli, C. Scopetani, D. Chelazzi, T. Martellini, M. Pogojeva and J. Slobodnik, *Sci. Total Environ.*, 2021, **760**, 143898.
47 F. Corradini, F. Casado, V. Leiva, E. Huerta-Lwanga and V. Geissen, *Sci. Total Environ.*, 2021, **752**, 141917.
48 R. Chand, L. A. Rasmussen, S. Tumlin and J. Vollertsen, *Sci. Total Environ.*, 2021, **798**, 149287.
49 E. Uurasjärvi, E. Sainio, O. Setälä, M. Lehtiniemi and A. Koistinen, *Environ. Pollut.*, 2021, **288**, 117780.
50 T. Pegado, L. Brabo, K. Schmid, F. Sarti, T. T. Gava, J. Nunes, D. Chelazzi, A. Cincinelli and T. Giarrizzo, *Mar. Pollut. Bull.*, 2021, **162**, 111799.
51 L. Wilkie Johnston, E. Bergami, E. Rowlands and C. Manno, *R. Soc. Open Sci.*, 2023, **10**, 221421.
52 L. A. Rasmussen, L. Iordachescu, S. Tumlin and J. Vollertsen, *Water Res.*, 2021, **201**, 117307.
53 S. Kernchen, M. G. Löder, F. Fischer, D. Fischer, S. R. Moses, C. Georgi, A. C. Nölscher, A. Held and C. Laforsch, *Sci. Total Environ.*, 2022, **818**, 151812.
54 J.-W. Jung, S. Kim, Y.-S. Kim, S. Jeong and J. Lee, *Sci. Total Environ.*, 2022, **825**, 154015.
55 L. Roscher, A. Fehres, L. Reisel, M. Halbach, B. Scholz-Böttcher, M. Gerriets, T. H. Badewien, G. Shiravani, A. Wurpts and S. Primpke, *Environ. Pollut.*, 2021, **288**, 117681.
56 L. Roscher, M. Halbach, M. T. Nguyen, M. Hebeler, F. Luschtinetz, B. M. Scholz-Böttcher, S. Primpke and G. Gerdts, *Sci. Total Environ.*, 2022, **817**, 152619.
57 B. V. Kumar, L. A. Löschel, H. K. Imhof, M. G. Löder and C. Laforsch, *Environ. Pollut.*, 2021, **269**, 116147.
58 S. M. Abel, S. Primpke, I. Int-Veen, A. Brandt and G. Gerdts, *Environ. Pollut.*, 2021, **269**, 116095.

59 K. Sipps, G. Arbuckle-Keil, R. Chant, N. Fahrenfeld, L. Garzio, K. Walsh and G. Saba, *Sci. Total Environ.*, 2022, **817**, 152812.
60 Y.-I. Kim, E. Jeong, J.-Y. Lee, R. W. Chia and M. Raza, *Environ. Res.*, 2023, **226**, 115682.
61 M. K. de Guzman, M. Andjelković, V. Jovanović, J. Jung, J. Kim, L. A. Dailey, A. Rajković, B. De Meulenaer and T. Ć. Veličković, *Mar. Pollut. Bull.*, 2022, **181**, 113846.
62 A. Jakobs, E. Gürkal, J. N. Möller, M. G. Löder, C. Laforsch and T. Lueders, *Sci. Total Environ.*, 2023, **857**, 159610.
63 X. Zhang, H. Wang, S. Peng, J. Kang, Z. Xie, R. Tang, Y. Xing, Y. He, H. Yuan, C. Xie and Y. Liu, *Front. Public Health*, 2022, **10**, 1005535.
64 P. Liu, L. Shao, Y. Li, T. Jones, Y. Cao, C. X. Yang, M. Zhang, M. Santosh, X. Feng and K. BéruBé, *Sci. Total Environ.*, 2022, **838**, 155989.
65 E. Lim, H. Tanaka, Y. Ni, Y. Bai and K. Ito, *Japan Architectural Review*, 2022, **5**, 682–690.
66 N. A. Forster, S. C. Wilson and M. K. Tighe, *J. Environ. Manage.*, 2023, **331**, 117304.
67 J. Nizamali, S. M. Mintenig and A. A. Koelmans, *J. Hazard. Mater.*, 2023, **441**, 129942.
68 L. Huan, Z. Long, M. Mindong, W. Haiwen, A. Lihui and Y. Zhanhong, *Sci. Total Environ.*, 2023, **867**, 161553.
69 S. Samandra, O. J. Mescall, K. Plaisted, B. Symons, S. Xie, A. V. Ellis and B. O. Clarke, *Sci. Total Environ.*, 2022, **837**, 155329.
70 H. Mu, Y. Wang, H. Zhang, F. Guo, A. Li, S. Zhang, S. Liu and T. Liu, *Sci. Total Environ.*, 2022, **839**, 156318.
71 S. Samandra, J. M. Johnston, J. E. Jaeger, B. Symons, S. Xie, M. Currell, A. V. Ellis and B. O. Clarke, *Sci. Total Environ.*, 2022, **802**, 149727.
72 P. S. Bäuerlein, R. C. H. M. Hofman-Caris, E. N. Pieke and T. L. ter Laak, *Water Res.*, 2022, **221**, 118790.
73 X. Tian, F. Beén and P. S. Bäuerlein, *Environ. Res.*, 2022, **212**, 113569.
74 L. Mughini-Gras, R. Q. J. van der Plaats, P. W. J. J. van der Wielen, P. S. Bauerlein and A. M. de Roda Husman, *Water Res.*, 2021, **192**, 116852.
75 L. An, T. Cui, Y. Zhang and H. Liu, *Sci. Total Environ.*, 2022, **847**, 157461.
76 J. Wu, Q. Ye, L. Sun, J. Liu, M. Huang, T. Wang, P. Wu and N. Zhu, *Sci. Total Environ.*, 2023, **879**, 163066.
77 Q. T. Whiting, K. F. O'Connor, P. M. Potter and S. R. Al-Abed, *Anal. Bioanal. Chem.*, 2022, **414**, 8353–8364.
78 Y. Fan, J. Zheng, L. Deng, W. Rao, Q. Zhang, T. Liu and X. Qian, *Water Res.*, 2022, **212**, 118116.
79 M. Bao, Q. Huang, Z. Lu, F. Collard, M. Cai, P. Huang, Y. Yu, S. Cheng, L. An, A. Wold and G. W. Gabrielsen, *Environ. Sci. Pollut. Res.*, 2022, **29**, 56525–56534.
80 Y. Tian, Z. Chen, J. Zhang, Z. Wang, Y. Zhu, P. Wang, T. Zhang, J. Pu, H. Sun and L. Wang, *J. Hazard. Mater.*, 2021, **407**, 124861.
81 P. S. Bäuerlein, E. N. Pieke, F. I. H. M. Oesterholt, T. Ter Laak and S. A. E. Kools, *Water Sci. Technol.*, 2023, **87**, 39–56.
82 L. Deng, H. Xi, C. Wan, L. Fu, Y. Wang and C. Wu, *J. Hazard. Mater.*, 2023, **451**, 131199.
83 M. Ourgaud, N. N. Phuong, L. Papillon, C. Panagiotopoulos, F. Galgani, N. Schmidt, V. Fauvelle, C. Brach-Papa and R. Sempéré, *Environ. Sci. Technol.*, 2022, **56**, 9999–10009.
84 L. Hildebrandt, F. El Gareb, T. Zimmermann, O. Klein, A. Kerstan, K. C. Emeis and D. Pröfrock, *Environ. Pollut.*, 2022, **307**, 119547.
85 X. Lu, H. He, Y. Wang, Y. Guo and X. Fei, *J. Hazard. Mater.*, 2023, **445**, 130542.
86 N. Liu, S. Cheng, X. Wang, Z. Li, L. Zheng, Y. Lyu, X. Ao and H. Wu, *Water Res.*, 2022, **226**, 119293.
87 W. Jia, A. Karapetrova, M. Zhang, L. Xu, K. Li, M. Huang, J. Wang and Y. Huang, *Sci. Total Environ.*, 2022, **844**, 156853.
88 Q. Li, A. Zeng, X. Jiang and X. Gu, *J. Hazard. Mater.*, 2021, **412**, 125164.
89 Y. Zhang, Y. Peng, C. Peng, P. Wang, Y. Lu, X. He and L. Wang, *Environ. Sci. Technol.*, 2021, **55**, 13802–13811.
90 A. López-Rosales, J. Andrade, V. Fernández-González, P. López-Mahía and S. Muniategui-Lorenzo, *Mar. Pollut. Bull.*, 2022, **178**, 113591.
91 X. Zhang, Y. He, Z. Xie, S. Peng, C. Xie, H. Wang, L. Liu, J. Kang, H. Yuan and Y. Liu, *Medicine*, 2022, **101**, E30215.
92 L. Zhu, J. Zhu, R. Zuo, Q. Xu, Y. Qian and L. An, *Sci. Total Environ.*, 2023, **856**, 159060.
93 S. Liu, G. Lin, X. Liu, R. Yang, H. Wang, Y. Sun, B. Chen and R. Dong, *Sci. Total Environ.*, 2023, **854**, 158699.
94 L. Qiu, W. Lu, C. Tu, X. Li, H. Zhang, S. Wang, M. Chen, X. Zheng, Z. Wang, M. Lin, Y. Zhang, C. Zhong, S. Li, Y. Liu, J. Liu and Y. Zhou, *Environ. Sci. Technol.*, 2023, **57**, 2435–2444.
95 S. Huang, X. Huang, R. Bi, Q. Guo, X. Yu, Q. Zeng, Z. Huang, T. Liu, H. Wu, Y. Chen, J. Xu, Y. Wu and P. Guo, *Environ. Sci. Technol.*, 2022, **56**, 2476–2486.
96 C. K. Chen, J. Zhang, A. Bhingarde, T. Matotek, J. Barrett, B. D. Hardesty, M. M. Banaszak Holl and B. L. Khoo, *Chem. Eng. J.*, 2022, **428**, 132614.
97 F. Yan, X. Wang, H. Sun, Z. Zhu, W. Sun, X. Shi, J. Zhang, L. Zhang, X. Wang, M. Liu, M. Cai and Y. Zhang, *Front. Mar. Sci.*, 2022, **9**, 845062.
98 H. Luo, Y. Zeng, Y. Zhao, Y. Xiang, Y. Li and X. Pan, *J. Hazard. Mater.*, 2021, **413**, 125342.
99 H. Luo, Y. Xiang, Y. Li, Y. Zhao and X. Pan, *J. Hazard. Mater.*, 2021, **404**, 124159.
100 M. G. Löder, H. K. Imhof, M. Ladehoff, L. A. Löschel, C. Lorenz, S. Mintenig, S. Piehl, S. Primpke, I. Schrank and C. Laforsch, *Environ. Sci. Technol.*, 2017, **51**, 14283–14292.
101 S. Wang, X. Tan, Y. Wu, J. Zhang, Z. Tian and J. Ma, *J. Hazard. Mater.*, 2024, **463**, 132840.
102 M. Kohantorabi, G. Moussavi and S. Giannakis, *Chem. Eng. J.*, 2021, **411**, 127957.
103 A. Spadea, J. Denbigh, M. J. Lawrence, M. Kansiz and P. Gardner, *Anal. Chem.*, 2021, **93**, 3938–3950.
104 J. Chae, S. An, G. Ramer, V. Stavila, G. Holland, Y. Yoon, A. A. Talin, M. Allendorf, V. A. Aksyuk and A. Centrone, *Nano Lett.*, 2017, **17**, 5587–5594.

105 S. Rizevsky, K. Zhaliazka, T. Dou, M. Matveyenka and D. Kurouski, *J. Phys. Chem. C*, 2022, **126**, 4157–4162.
106 M. G. J. Löder, M. Kuczera, S. Mintenig, C. Lorenz and G. Gerdts, *Environ. Chem.*, 2015, **12**, 563–581.
107 P. Bassan, H. J. Byrne, F. Bonnier, J. Lee, P. Dumas and P. Gardner, *Analyst*, 2009, **134**, 1586–1593.
108 A. Kohler, J. Sule-Suso, G. Sockalingum, M. Tobin, F. Bahrami, Y. Yang, J. Pijanka, P. Dumas, M. Cotte and D. Van Pittius, *Appl. Spectrosc.*, 2008, **62**, 259–266.
109 S. Primpke, R. K. Cross, S. M. Mintenig, M. Simon, A. Vianello, G. Gerdts and J. Vollertsen, *Appl. Spectrosc.*, 2020, **74**, 1127–1138.